Hindawi
Advances in Meteorology
Volume 2019, Article ID 8709575, 14 pages
https://doi.org/10.1155/2019/8709575

Research Article

Fusion of Simulated and Observational Temperature Data in the Beijing-Tianjin-Hebei Region Based on High-Accuracy Surface Modeling

Yu Liu,[1,2] **Tianxiang Yue**,[1,2] **Yimeng Jiao**,[3] **Yapeng Zhao**,[1,2] **and Zhengyi Bao**[1,2]

[1]*State Key Laboratory of Resources and Environmental Information System, Institute of Geographic Sciences and Natural Resources Research, Chinese Academy of Sciences, Beijing 100101, China*
[2]*University of Chinese Academy of Sciences, Beijing 100049, China*
[3]*School of Earth Sciences and Resources, China University of Geosciences (Beijing), Beijing 100083, China*

Correspondence should be addressed to Yu Liu; liuyu.15b@igsnrr.ac.cn

Received 8 October 2018; Accepted 5 March 2019; Published 27 March 2019

Academic Editor: Roberto Coscarelli

Temperature changes have a major impact on all aspects of human society and have attracted global attention. The scarcity of observation data and the inaccuracy of the models make obtaining accurate temperature distributions a challenge. This study introduces high-accuracy surface modeling (HASM) combined with temperature simulations from the Weather Research and Forecasting (WRF) model and temperature records from observation stations to investigate the spatiotemporal characteristics of temperature in the Beijing-Tianjin-Hebei region during the period of 1956–2005. Leave-one-out cross-validation is applied to verify the temperature fields before and after the fusion of the models. The results indicate that the WRF model has a limited ability to simulate temperature conditions, but the overall deviation across the region is relatively large. The fusion results of the HASM decrease the mean absolute error (MAE) and the root-mean-square error (RMSE) by half in most instances, and the correlation between the fusion data and observation data is approximately 0.01–0.03 higher than that with the WRF simulation data. Based on the fusion data, obvious warming trends are observed during 1976–2005. In general, temperatures in spring, summer, and autumn increase rapidly from 1996 to 2005 but from 1976 to 1995 in winter. The substantial fluctuations in the interannual temperature during 1996–2005 in summer, autumn, and winter may be related to the frequent occurrence of extreme weather. The spatial distribution of temperature change differs in each season during 1956–1995. A dramatic increase in temperature occurs in the western part of the study area during 1996–2005 but with no seasonal difference.

1. Introduction

The impact of human activities on the natural environment has led to global and regional climate change, which has a major impact on all aspects of human society, such as the economy, agriculture, fishing industry, hydraulic engineering, and relevant policymaking [1–4]. Temperature is the most direct meteorological factor for the characterization of climate change. The Intergovernmental Panel on Climate Change (IPCC) fifth report [5] noted that the warming rate at the global scale reached 0.12°C/10 yr from 1951 to 2012, which was accompanied by fewer cold days and nights and more warm days and nights. At the same time, extreme high/low-temperature weather and hydrological disasters, such as droughts and floods, occur frequently all over the world.

Human activities, such as urbanization and returning farmlands to forests, can greatly change the land cover, and greenhouse gas emissions from industrial activity, vehicles, and heating in winter can increase the concentration of greenhouse gas in the air; both of these activities drive climate change. There are also regional differences in climate change due to differences in human aggregation and activity [6–9]. China is a populous country with a fast-growing economy. From 1989 to 2018, China's gross domestic product (GDP) grew at an average annual rate of 9.55% [10],

and the population also grew rapidly [11]. In the Beijing-Tianjin-Hebei region, which is the political, economic, and cultural center of China and an urban agglomeration, land cover has changed dramatically in recent decades. Factors, such as urban expansion, farmland reduction, artificial vegetation, greenhouse gas emissions, aerosol changes, and the heat island effect, have large impacts on the climate in this region. These influences also affect socioeconomic factors such as people's livelihood and security [12, 13]. Studying the climate change characteristics of the Beijing-Tianjin-Hebei region also provides a basis for the formulation of relevant policies [14].

Many studies on spatiotemporal temperature patterns have been conducted in the Beijing-Tianjin-Hebei region. Yan et al. [15] integrated observation data from the Beijing Observatory Station and reported that the observed temperature data of the station were likely to be approximately 0.48°C/10 yr. Li and Yao [16] performed an inhomogeneity analysis for observation data using the Multiple Analysis of Series for Homogenization (MASH) software package. Zhao et al. [17] used 327 observation stations to explore the temporal and spatial variations in temperature in the Beijing-Tianjin-Hebei region for 50 years and found that the annual temperature over 10 years largely changed in the southeast and that interdecadal variations of temperature were spatially stationary and varied from −0.05°C to 0.05°C. Because of the spatial discontinuity of the observed dataset, regional weather models have also been used to study climate change. For instance, Miao et al. [18] used the Weather Research and Forecasting (WRF) model to study the effects of urbanization on surface weather and the boundary layer structure and found that the urban canopy variables simulated by the model were in good agreement with the ground observations. Liu et al. [19] ran sensitivity tests on the regional weather model and suggested that heat waves enhanced urban warming intensity at night. Based on the Regional Climate Model version 3 (RegCM3), Zhang and Shi [20] studied the changes in precipitation, temperature, and certain related extreme weather events in northern China under the background of global warming. However, limited by the lack of understanding of atmospheric motion and human activities, biases remain in the results of the numerical weather models [21, 22].

The objective of this paper is to perform the high-accuracy surface modeling (HASM) to fuse the observation data from stations and the simulations from numerical weather models. At present, there is no study using a dynamical downscaling model as the input conditions of HASM to simulate the surface temperature. The previous studies performed statistical downscaling such as Bayesian statistical methods, linear regression methods, interpolation, and geographical weighted regression to produce the input conditions of HASM [17, 23–25]. From the mechanism of temperature distribution, a dynamical downscaling model has more realistic and reliable results [26] and improves the accuracy of the final results of HASM. We use the WRF model to downscale the Community Earth System Model (CESM) climate data from 1956 to 2005 and apply these data to drive the HASM. Then, the time continuous observation data of the Beijing-Tianjin-Hebei region during the study period are screened and used as the accuracy control conditions of HASM. By running HASM, we obtain the fused temperature fields and compare the accuracy of the temperature data before and after the fusion. Finally, the temporal and spatial variations in temperature in the Beijing-Tianjin-Hebei region from 1956 to 2005 are analyzed based on the HASM fusion results.

2. Data and Methods

2.1. Study Region. The location of the Beijing-Tianjin-Hebei region is shown in Figure 1(a) (between 36°N–42.5°N and 113°E–120°E). This region incorporates Beijing, Tianjin, and Hebei Provinces. Beijing and Tianjin have high levels of urbanization, and the central areas of these two cities are dominated by underlying urban areas. The elevation of Hebei Province is high in the northwest and low in the southeast, with complex and diverse landforms. Population is mostly distributed in the low-elevation area, where the land cover is dominated by cities and farmland. The northwest region of Hebei Province is covered by mountain forests and grasslands. The Beijing-Tianjin-Hebei region is a key economic zone in China that is affected by climate change and, in turn, influences the trend of climate change due to its large population and the change in land cover. Therefore, studying the temporal and spatial changes in temperature in the Beijing-Tianjin-Hebei region can improve our understanding of the relationship between climate change and the local ecological environment.

2.2. Observation Data. We obtained long-term (1956–2005) air temperature records from meteorological observation stations within and outside of the Beijing-Tianjin-Hebei region from the National Meteorological Information Center. Based on the HASM calculation, the additional data around the study area can significantly improve the HASM result [27]. After screening, 64 stations with continuous observations met the research requirements during the study period (Figure 1(b)). Among them, 26 observation stations are located in the Beijing-Tianjin-Hebei region and 38 are distributed around the region. The air temperature records are processed into monthly means.

2.3. WRF. As a next-generation mesoscale numerical weather prediction system, the WRF model has been widely applied in climate research [28, 29]. Version 3.5.1 of the WRF model is utilized in this paper to produce long-term (1956–2005) temperature simulations. The initial and boundary conditions for the simulations are the global bias-corrected climate model output data from version 1 of the National Center for Atmospheric Research (NCAR) CESM (CESM1), which participated in the Coupled Model Intercomparison Experiment Phase 5 (CMIP5). This dataset was produced to support the simulations of the WRF model with 26 pressure levels and 6 hourly intervals. From 1981 to 2005, a bias-correction [30] was implemented to the dataset

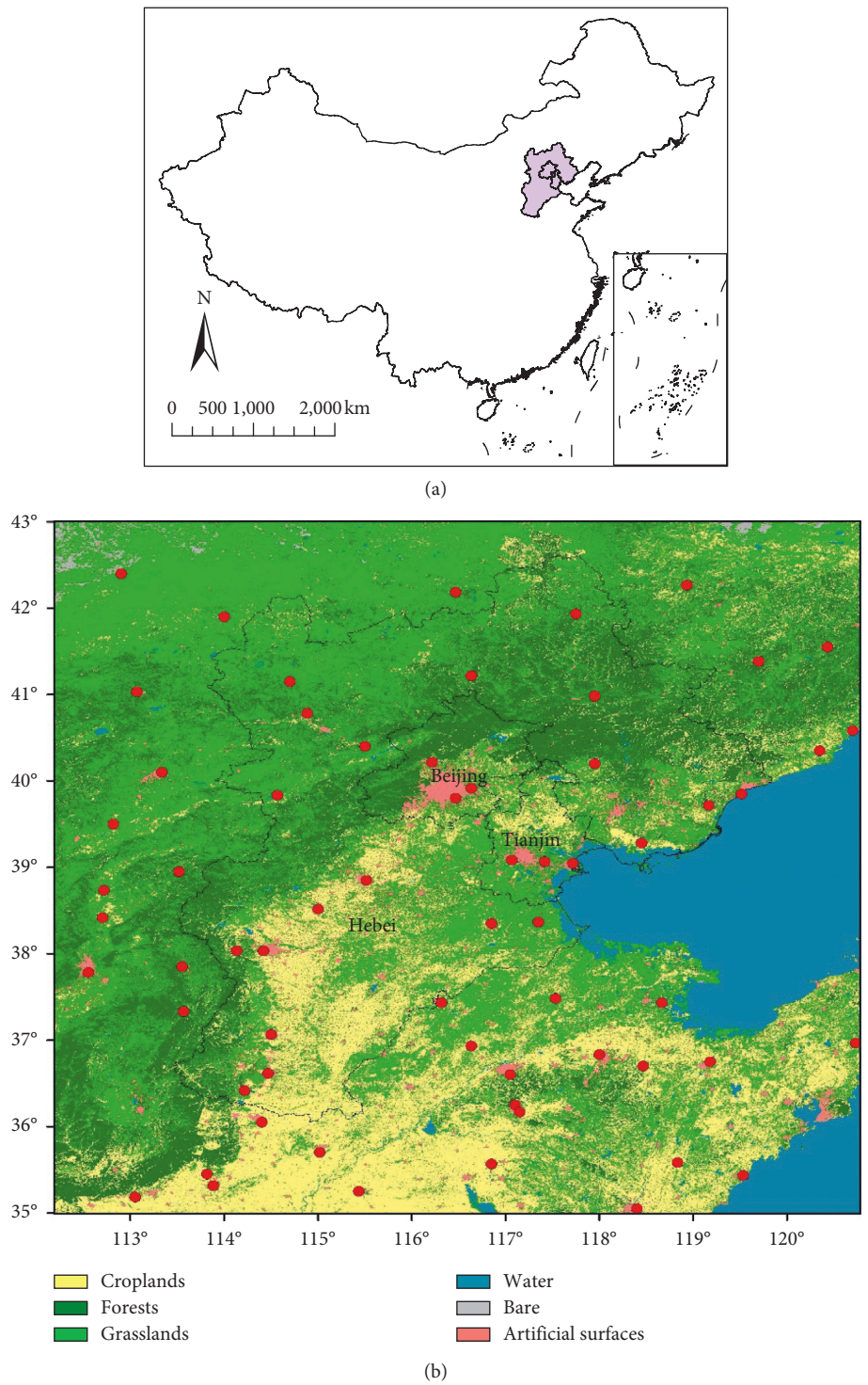

Figure 1: Study region: (a) location of the Beijing-Tianjin-Hebei region in China; (b) land cover of the study region derived from the European Space Agency (ESA) global land cover dataset. The red dots represent the locations of the available observation stations during the study period (1956 to 2005).

using the European Centre for Medium-Range Weather Forecasts (ECMWF) Interim Reanalysis (ERA-Interim).

Numerous parameterization options are selected, such as the Yonsei University (YSU) boundary layer scheme, Monin–Obukhov surface-layer scheme, WRF single-moment (WSM) 6-class Graupel scheme, rapid radiative transfer model (RRTM) longwave radiation scheme, Goddard shortwave radiation scheme, unified Noah land-surface process scheme, and Kain–Fritsch (new Eta) cumulus scheme. The WSM6 microphysics was included primarily to provide useful

information on high-resolution weather phenomena and are competitive options for use in WRF by reproducing precipitating convection and associated meteorological phenomena such as air temperature [31]. We set the WRF model to output and process the hourly simulations into monthly values consistent with the processed observation data.

2.4. HASM. The geometric properties of a surface, such as the lengths of curves, the angles of tangent vectors, the areas of regions, and the geodesics on surfaces, are called the first fundamental coefficients of the surface. The local deformations of the surface, such as the deviations in the relevant points on the surface from the tangent plane, are called the second fundamental coefficients of the surface. The first and second fundamental coefficients are also called intrinsic and extrinsic invariants, respectively, because the former is usually measured from outside of the surface and the latter is measured on the surface [32]. According to the fundamental theorem of surface, the first and second fundamental coefficients uniquely identify a surface. HASM is developed based on this theory.

A surface, z, is defined as $z = f(x, y)$. The first and second fundamental coefficients of the surface z are defined as follows:

$$E = 1 + f_x^2, \tag{1}$$

$$F = f_x \cdot f_y, \tag{2}$$

$$G = 1 + f_y^2, \tag{3}$$

$$L = \frac{f_{xx}}{\sqrt{1 + f_x^2 + f_y^2}}, \tag{4}$$

$$M = \frac{f_{xy}}{\sqrt{1 + f_x^2 + f_y^2}}, \tag{5}$$

$$N = \frac{f_{yy}}{\sqrt{1 + f_x^2 + f_y^2}}, \tag{6}$$

where equations (1)–(3) and (4)–(6) determine the first and second fundamental coefficients, respectively. f_x denotes the first-order partial derivative of the surface z with respect to the independent variable x. f_{xx} denotes the second-order partial derivative of the surface z with respect to the independent variable x. f_y, f_{yy}, and f_{xy} are defined similarly.

Following the Gauss–Codazzi equations, the first fundamental coefficients (equations (1)–(3)) and the second fundamental coefficients (equations (4)–(6)) can be related as follows:

$$f_{xx} = \Gamma_{11}^1 f_x + \Gamma_{11}^2 f_y + \frac{L}{\sqrt{E + G - 1}}, \tag{7}$$

$$f_{xy} = \Gamma_{12}^1 f_x + \Gamma_{12}^2 f_y + \frac{M}{\sqrt{E + G - 1}}, \tag{8}$$

$$f_{yy} = \Gamma_{22}^1 f_x + \Gamma_{22}^2 f_y + \frac{N}{\sqrt{E + G - 1}}, \tag{9}$$

where

$$\begin{aligned}
\Gamma_{11}^1 &= \frac{GE_x - 2FF_x + FE_y}{2(EG - F^2)}, \\
\Gamma_{12}^1 &= \frac{GE_x - FG_x}{2(EG - F^2)}, \\
\Gamma_{22}^1 &= \frac{2GF_y - GG_x - FG_y}{2(EG - F^2)}, \\
\Gamma_{11}^2 &= \frac{2EF_x - EE_y - FE_x}{2(EG - F^2)}, \\
\Gamma_{12}^2 &= \frac{EG_x - FE_y}{2(EG - F^2)}, \\
\Gamma_{22}^2 &= \frac{EG_y - 2FF_y + FG_x}{2(EG - F^2)}.
\end{aligned} \tag{10}$$

In the definition of HASM, equations (7)–(9) are used to build the computational formula as follows:

$$\begin{cases}
\min \left\| \begin{bmatrix} A \\ B \\ C \end{bmatrix} \cdot z^{(n-1)} - \begin{bmatrix} d \\ q \\ h \end{bmatrix}^{(n)} \right\|_2, \\
S \cdot z^{(n-1)} = k,
\end{cases} \tag{11}$$

where A, B, and C represent equations (7)–(9) in the coefficient matrix, respectively. d, q, and h represent equations (7)–(9) in the right-hand vector, respectively, and n represents the number of iterations. $S \cdot z^{(n-1)} = k$ is used to introduce the observation information into the surface, which is determined by the first equation of equation set (11). S denotes the sampling matrix, and k denotes the sampling vector.

HASM has been applied in multiple research fields on global and regional scales [33–41]. In the most recent research, the driving fields of HASM are created by statistical methods that usually lack the dynamic interpretation of the distribution of quantities and result in deviations in non-observation points. Therefore, the WRF model is applied in this paper to compensate for deficiency in the statistical method by dynamically downscaling the coarse-resolution CESM1 results.

3. Results and Discussion

3.1. Precision Test. The observations from 26 stations located in the Beijing-Tianjin-Hebei region are chosen as the true values to test the accuracy of the temperature fields from the WRF simulation and the updated temperature fields after HASM fusion. Because the observations enter the HASM calculation as the accuracy control conditions, it is not appropriate to directly use the temperature observation data to verify the accuracy of the updated temperature field.

Therefore, we use the leave-one-out cross-validation method to test the accuracy of the HASM calculation results. That is, one point is extracted from 26 stations as the test point, and the other 25 points together with the 38 points outside the Beijing-Tianjin-Hebei region are input into the HASM calculation as the accuracy control conditions. The fusion accuracy of the HASM is verified by comparing the observations with the HASM output at the test point. The leave-one-out cross-validation is repeated 26 times until each of the 26 observation points serves as the test point once.

According to the meteorological definition, the 12 months of the year are divided into four seasons: spring (March to May), summer (June to August), autumn (September to November), and winter (December to February). Figures 2(a)–2(h) show the distribution of the bias in the seasonal mean temperature in the WRF simulations and HASM fusion results compared to the observations in 1956–2005. The WRF simulations in spring, autumn, and winter are significantly higher than the temperature observations, and the deviations along the west side of the study area are higher than those along the east side. In summer, the WRF model shows significantly better simulation results, with only a warm bias in the middle of the study area (higher than 0.5°C) and a cool bias in the northeast (lower than −0.5°C), which is accompanied by a deviation between 0.5°C and −0.5°C in other areas. The cross-validation shows that the accuracy of the HASM fusion results is significantly improved compared with that of the WRF model; not only is the number of high-deviation sites significantly reduced, but the degree of deviation is greatly decreased. In spring, autumn, and winter, the warm deviations in the WRF simulation in the western part of the study area are eliminated. Five stations in Tianjin and south of Tianjin improve in spring and autumn, whereas in winter, two of the five stations transform into cool biases. At the same time, during these three seasons, HASM has limited optimization ability in the northern part of the study area. The point on the northernmost side of the study area changed from a weak deviation in the WRF model to a cool deviation in the HASM (lower than −1°C). The reason may be that the estimation of nonobservation points in the HASM requires information from the surrounding observation points. However, in this case, the observation stations around this northernmost point are sparse, and there is no observation point on its north side, resulting in an increase in the deviation of the point. Due to the high simulation accuracy of the WRF model in summer, the HASM output does not change substantially. The distribution of biases in the annual mean temperature is shown in Figures 2(i)–2(j). The WRF simulation value is significantly warmer than the observation value, and the degree of deviation gradually increases from southeast to northwest. HASM significantly improves the WRF simulation, and the deviations at most of the observation points are reduced, especially the positive deviations in the western part of the study area. Similarly, the two points located on the northernmost side and along the coast of Tianjin have an increased bias due to the lack of surrounding observations, which illustrates that a boundary problem exists in the HASM method.

To further quantify the accuracy, Tables 1–3 list the mean absolute error (MAE), root-mean-square error (RMSE), and spatial correlation coefficient (SCC) for the WRF-simulated temperature and HASM fusion results. The formulations of MAE, RMSE, and SCC are as follows:

$$\mathrm{MAE} = \frac{1}{n}\sum_{k=1}^{n}\left|o_k - s_k\right|, \tag{12}$$

$$\mathrm{RMSE} = \sqrt{\frac{1}{n}\sum_{k=1}^{n}\left(o_k - s_k\right)^2}, \tag{13}$$

$$\mathrm{SCC} = \frac{\sum_{i=1}^{n}\left(o_k - \overline{o_k}\right)\left(s_k - \overline{s_k}\right)}{\sqrt{\sum_{i=1}^{n}\left(o_k - \overline{o_k}\right)^2 \sum_{i=1}^{n}\left(s_k - \overline{s_k}\right)^2}}. \tag{14}$$

Tables 1 and 2 show that, after the observation data are fused, the accuracy of the HASM output is substantially higher than that of the original WRF simulation data. The deviations in the spring, autumn, winter, and annual means are reduced by at least half, and the RMSE is basically the same. At the same time, this result also reflects the high precision of the WRF simulation in summer in the Beijing-Tianjin-Hebei region, which has also been improved slightly by HASM. The calculation of MAE and RMSE is based on the bias (equations (12) and (13)); thus, the bias distribution in Figure 2 shows the MAE and RMSE between HASM and station data at different stations. The stations with greater biases have higher MAE and RMSE. The deviations of most stations in HASM are decreasing, which significantly reduces the MAE and RMSE of HASM. However, the observation station deviation on the northernmost side is continuously increasing in HASM; thus, there is a negative contribution to MAE and RMSE at this point.

In Table 3, the SCC indicates that the temperature fields before and after integration are the best in summer and autumn and slightly worse in spring and winter. The correlation between HASM fusion data and observation data is approximately 0.01–0.03 higher than that with the WRF simulation data for each season, and the average annual temperature correlation increases by 0.02. The SCC indicates the degree of coincidence between the simulations and the observations with respect to the spatial distribution characteristics. The variation is only 0.01–0.03 because the WRF is already highly accurate (at least 0.93 of SCC) and can simulate the spatial distribution of surface temperature very well. Although HASM has smaller MAE and RMSE, the spatial distribution characteristics of surface temperature simulated by HASM do not change greatly. From Figure 2, we can also see that, in a few stations, the biases increase, which also limits the improvement of the SCC of HASM compared with that of WRF.

Figure 3 compares the interannual change in average temperature bias at 26 points in the WRF simulation and HASM fusion. The difference in the WRF model and observations fluctuates greatly from −2°C to 2°C, which indicates strong instability in the WRF simulations. Since the numerical weather model is essentially an initial value problem, the simulation results are largely dependent on the

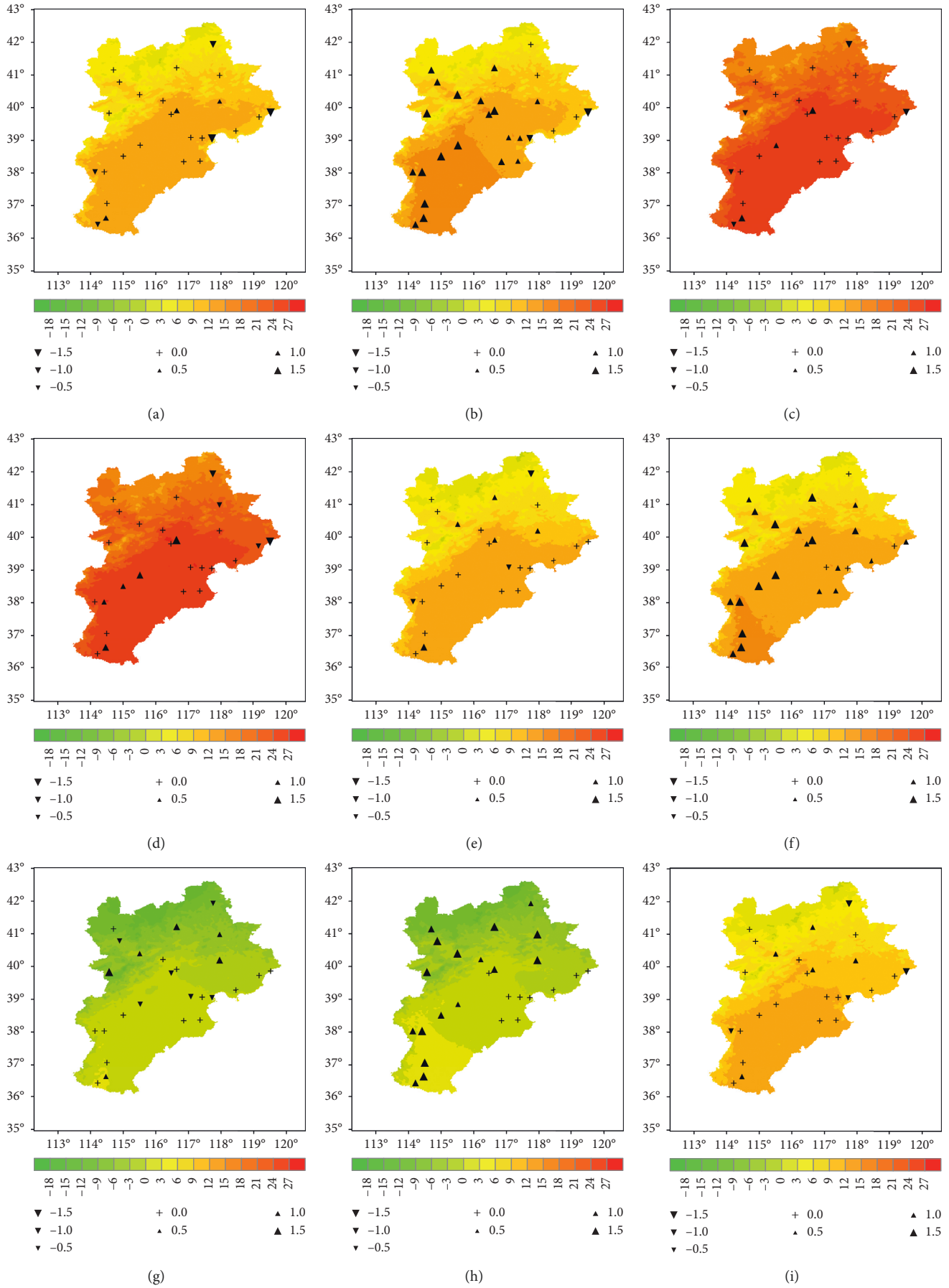

Figure 2: Continued.

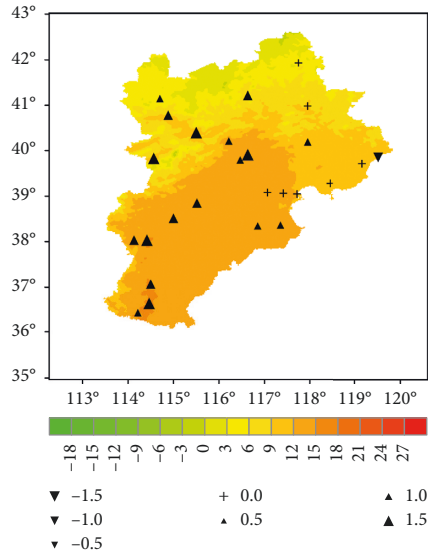

(j)

Figure 2: Distribution of the bias in the seasonal mean and annual mean temperature in the WRF simulation and HASM fusion compared to the observations in 1956–2005. ▲ denotes warm bias. ▼ denotes cool bias. (a) HASM-spring; (b) WRF-spring; (c) HASM-summer; (d) WRF-summer; (e) HASM-autumn; (f) WRF-autumn; (g) HASM-winter; (h) WRF-winter; (i) HASM-annual; (j) WRF-annual.

Table 1: Mean absolute error (MAE) values of the WRF model and HASM.

	SPR	SUM	AUT	WIN	ANN
WRF	1.35	0.54	1.13	1.25	0.99
HASM	0.55	0.40	0.42	0.61	0.41

Table 2: Root-mean-square error (RMSE) values of the WRF model and HASM.

	SPR	SUM	AUT	WIN	ANN
WRF	1.57	0.73	1.29	1.64	1.16
HASM	0.92	0.57	0.52	0.82	0.53

Table 3: Spatial correlation coefficient (SCC) values of the WRF model and HASM.

	SPR	SUM	AUT	WIN	ANN
WRF	0.93**	0.97**	0.97**	0.94**	0.96**
HASM	0.95**	0.98**	0.98**	0.97**	0.98**

**Passing the confidence test of 99%.

accuracy of the initial field. The initial field used in the WRF model in this paper was bias corrected from 1981 to 2005, but the temperature deviation in the WRF model from 1981 to 2005 was not significantly improved compared with that from 1956 to 1980. Therefore, the temperature deviation in the WRF-simulated data may not be inherited from the initial field but, rather, results from the misinterpretation of the atmospheric mechanism by the WRF model itself. Cross-validation shows that the HASM greatly reduces the bias, with a slight cold deviation of no more than −0.2°C. The seasonal temperature deviation characteristics are similar to those in Figure 3.

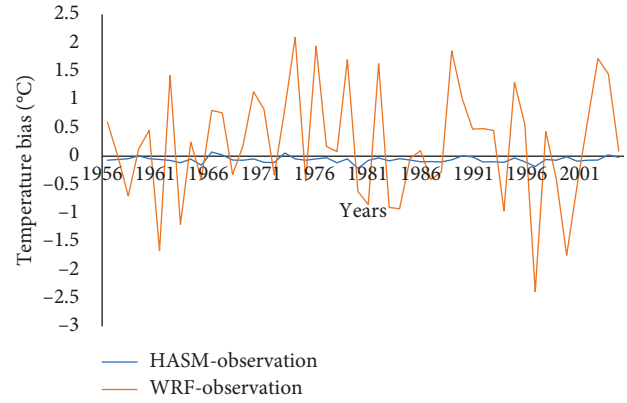

Figure 3: Interannual variability in the average temperature bias of the HASM and WRF data at 26 stations in the Beijing-Tianjin-Hebei region in 1956–2005.

In summary, the spatial and temporal accuracies of the HASM fusion results are significantly higher than those of the WRF simulation. The fusion data contain information on the temperature distribution mechanism from the WRF and correction information from the observation data, which is highly suitable for long-term sequential climate analyses. In the next section, we use the HASM fusion data to analyze the temporal and spatial variations in temperature in the Beijing-Tianjin-Hebei region from 1956 to 2005.

3.2. Trend Analysis of Temperature. The average temperatures of the Beijing-Tianjin-Hebei region are seasonally averaged, and their interannual variations are shown in Figure 4. The average regional temperature in the four seasons fluctuates and increases over time, but the heating rates are significantly different. In spring, the heating rate

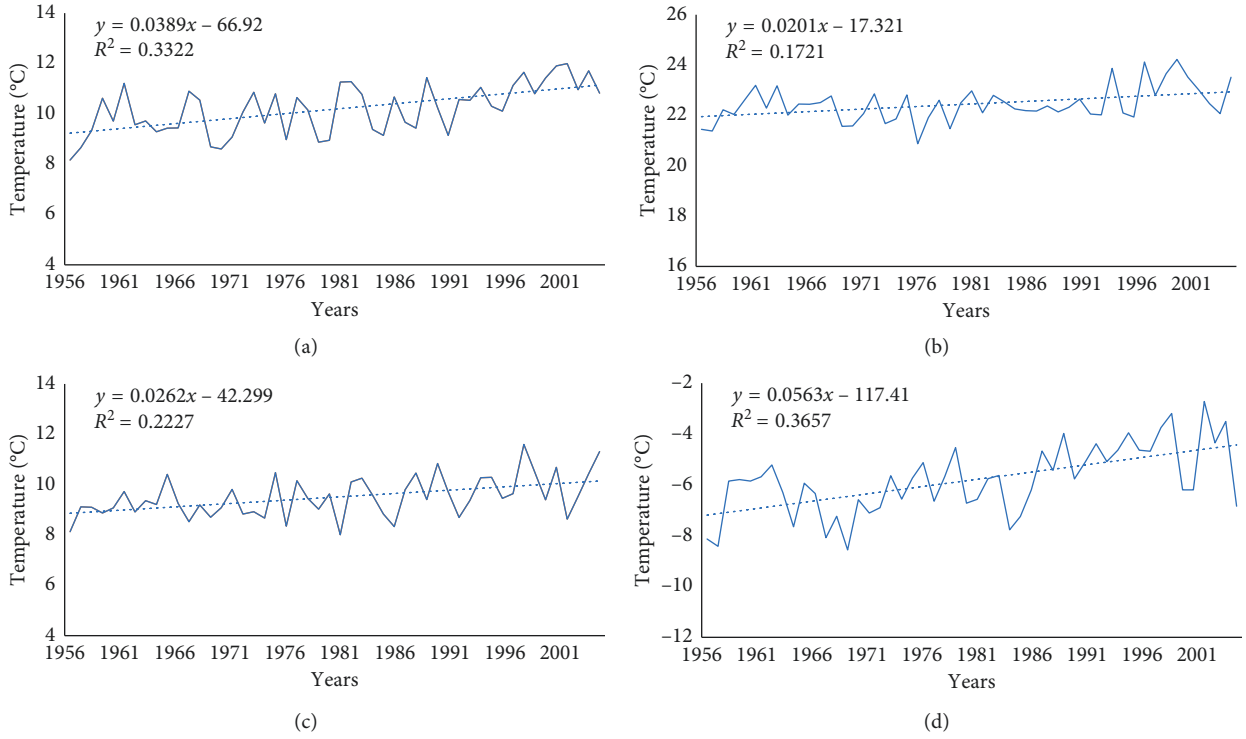

Figure 4: Interannual variation of seasonal mean temperature in the Beijing-Tianjin-Hebei region from 1981 to 2010: (a) spring; (b) summer; (c) autumn; (d) winter.

was approximately 0.039°C/yr; the regional average minimum temperature appeared at the beginning of the study period (8.2°C in 1956), and the highest temperature appeared in 2002 (12.0°C). The warming rate in summer decreased to 0.02°C/yr, with a maximum temperature of 20.9°C in 1976 and a minimum temperature of 24.2°C in 2000. The second lowest warming rate occurred in autumn at 0.026°C/yr. The lowest temperature in autumn was 8.1°C in 1956, and the highest temperature was 11.6°C in 1998. Winter exhibited the highest increasing temperature rate of the four seasons (0.056°C/yr). The lowest temperature occurred in 1969 (−8.6°C), and the highest temperature was −2.7°C in 2002. In the 50-year period, winter and spring have high rates of temperature changes. The temperature increases slowly in summer and autumn, but these rates are also higher than the global warming rate reported in IPCC5.

To further analyze the change in average temperature, we divide the study period into five periods: T1 (1956–1965), T2 (1966–1975), T3 (1976–1985), T4 (1986–1995), and T5 (1996–2005). Figure 5 shows the mean and variance in the decadal temperature over the five periods for each season, which characterize the temperature change between the five periods and the fluctuations in temperature during each period. In spring from T1 to T3, the average temperature increased slightly but fluctuated greatly, especially in the T3 period. From T4 to T5, the temperature increased rapidly, and the variance decreased, indicating that the interannual temperature changes were relatively stable. In summer, the temperature changes between the first four periods were less than 0.2°C and accompanied by slightly cooler temperatures in the T1–T3 period, and the interannual fluctuation in temperature was small. The main warming occurred from T4 to T5, and the average temperature increased above 0.7°C. However, during the T5 period, the interannual temperature was relatively unstable. The change in the average temperature in autumn was similar to that in spring. The first three periods experienced little change, and the temperature increased rapidly in T4 and T5, with a heating rate of 0.4°C/10 yr. Over time, the temperature in autumn gradually became unstable and the interannual changes increased. The temperature change in winter was much more complicated. After a brief cooling from T1 to T2, the T3, T4, and T5 periods heated up rapidly. The interannual temperature changes in each period also experienced a trend of decreasing first and then increasing dramatically in the T5 period.

Based on the above analysis, the four seasons reveal a rapid warming process from T3 to T5, which coincides with the period of rapid economic development after China's reform and opening policy. Except for spring, the regional average temperatures in summer, autumn, and winter have the largest variations during the T5 period, indicating that the temperature becomes unstable during this period, which may be related to the frequent occurrence of extreme weather in the context of global climate change. Zhai and Pan [42] studied the trend in temperature extremes in China and reported that, since the 1990s, the average numbers of warm days and warm nights exhibited increasing trends. Wang et al. [43] further confirmed that extreme temperature (highest and lowest) in North China, including the Beijing-

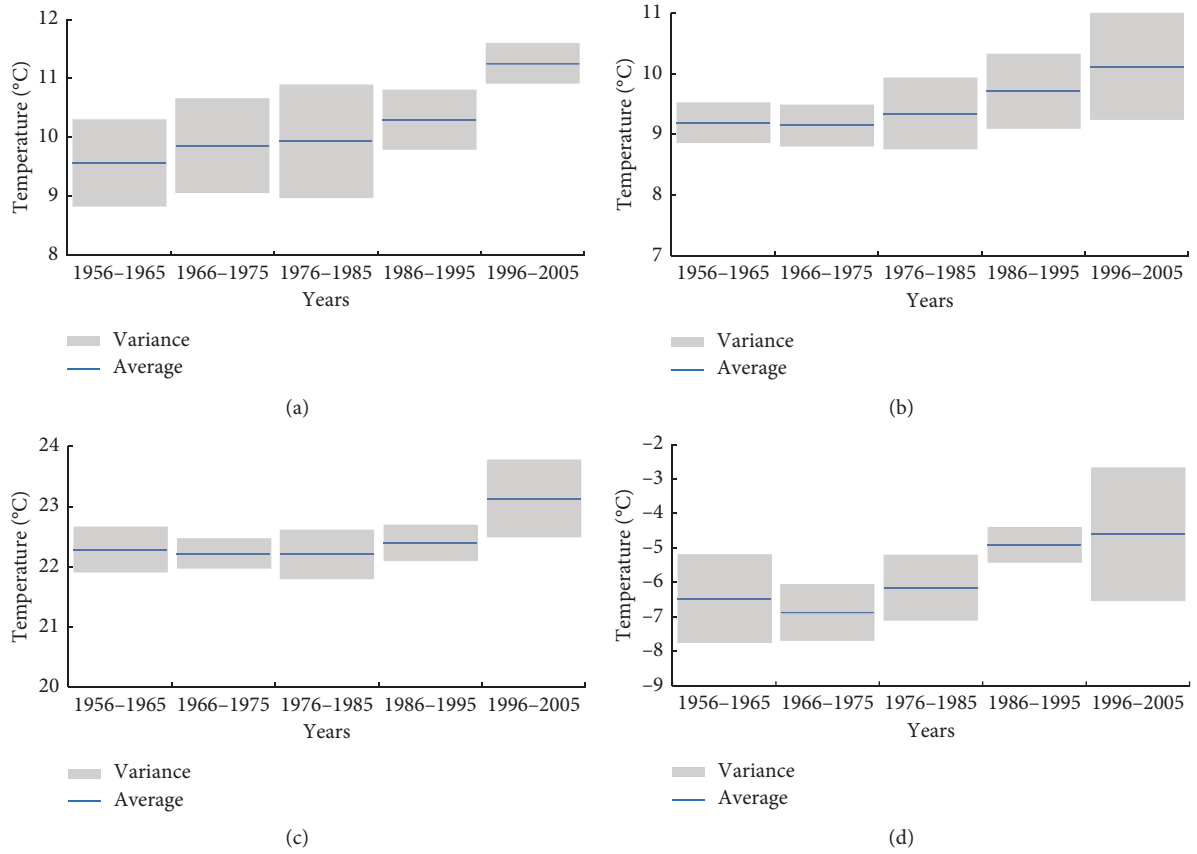

Figure 5: Decadal mean and variance of the regional average temperature for each season: (a) spring; (b) autumn; (c) summer; (d) winter.

Tianjin-Hebei region, showed a clear upward trend, and extreme warm events were much stronger than the extreme cold events.

Figure 6 shows the interannual variation in the annual mean temperature and the average temperature change over ten years. The overall warming rate of the annual mean during the study period reaches 0.035°C/yr, and the main warming period occurs in the last 20 years, with a heating rate greater than 0.55°C/10 yr. However, the decadal variation in temperature gradually decreases with time, which may be because the annual scale is too large, and the influence of extreme weather on temperature is smoothed out.

3.3. Spatial Distribution of Decadal Changes. In this section, the spatial distribution of temperature changes over time is analyzed. Following the definition in the previous section, the study period is still divided equally into five decades, the difference between two adjacent decades is calculated, and the spatial evolution of the 10-year average temperature is obtained.

Figure 7 shows the spatial distribution of the decadal temperature changes in spring and summer. The overall temperature in the region increases significantly from T1 to T2 and from T3 to T5 in spring and from T4 to T5 in summer, which matches the findings reported in Figure 5 well, but there are some differences in the spatial distribution of temperature changes between different time periods and seasons. In the spring from T1 to T2, the northern part of the Beijing-Tianjin-Hebei region is mainly cooled, with a cooling range from −0.2°C to 0°C. As the latitude decreases, the air gradually becomes warmer, and the maximum temperature increase occurs in the cities of Xingtai and Handan in the southern part of the study area, exceeding 0.6°C. The temperature distribution in the summer from T1 to T2 is similar to that in spring, but the temperature increase in the southern part of the study area is very weak. From T2 to T3, the spatial distribution and degree of temperature change in spring and summer are basically the same, showing the characteristics of slightly cooling in the south and warming in the north. From T3 to T4, the warming area covers the entire study area. In spring, the temperature rises to 0.4°C north and east of the study area and in Beijing and Tianjin (specifically, more than 0.6°C in the eastern part of Tianjin and the northeastern edge of Hebei Province). The temperature rise in this stage in summer is less than that in spring, with a small temperature increase of 0.4°C in the western part of the study area and Beijing. During the study period, the maximum temperature increase occurred during the T4 to T5 stage. In the spring, most areas warmed above 0.8°C, especially on the west side of the Beijing-Tianjin-Hebei region, where there was a large temperature increase of more than 1.2°C. The temperature change from T4 to T5 in summer was slightly less than that in spring, but the distribution was similar, and a strong warming area also appeared in the west.

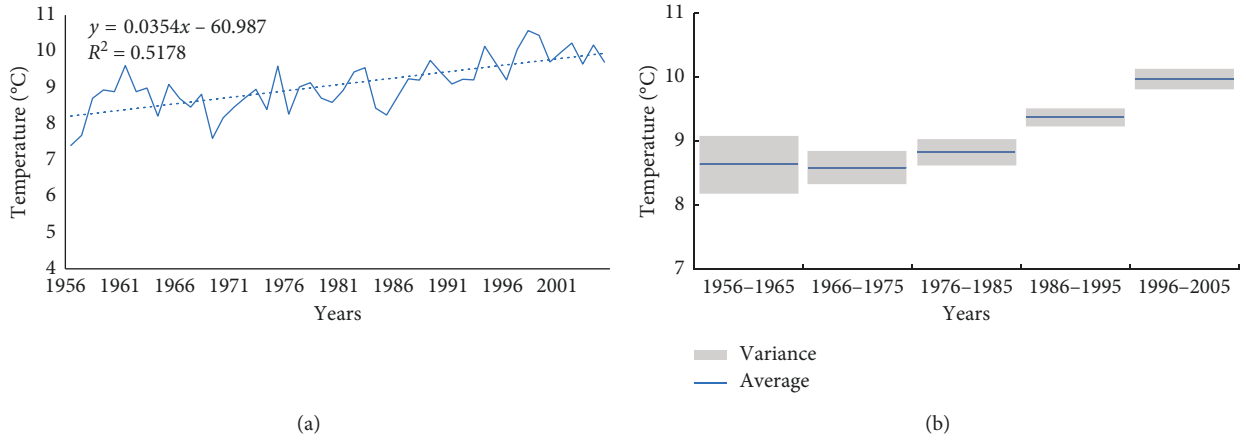

Figure 6: (a) Interannual variation in the annual mean temperature and (b) the average temperature change over ten years.

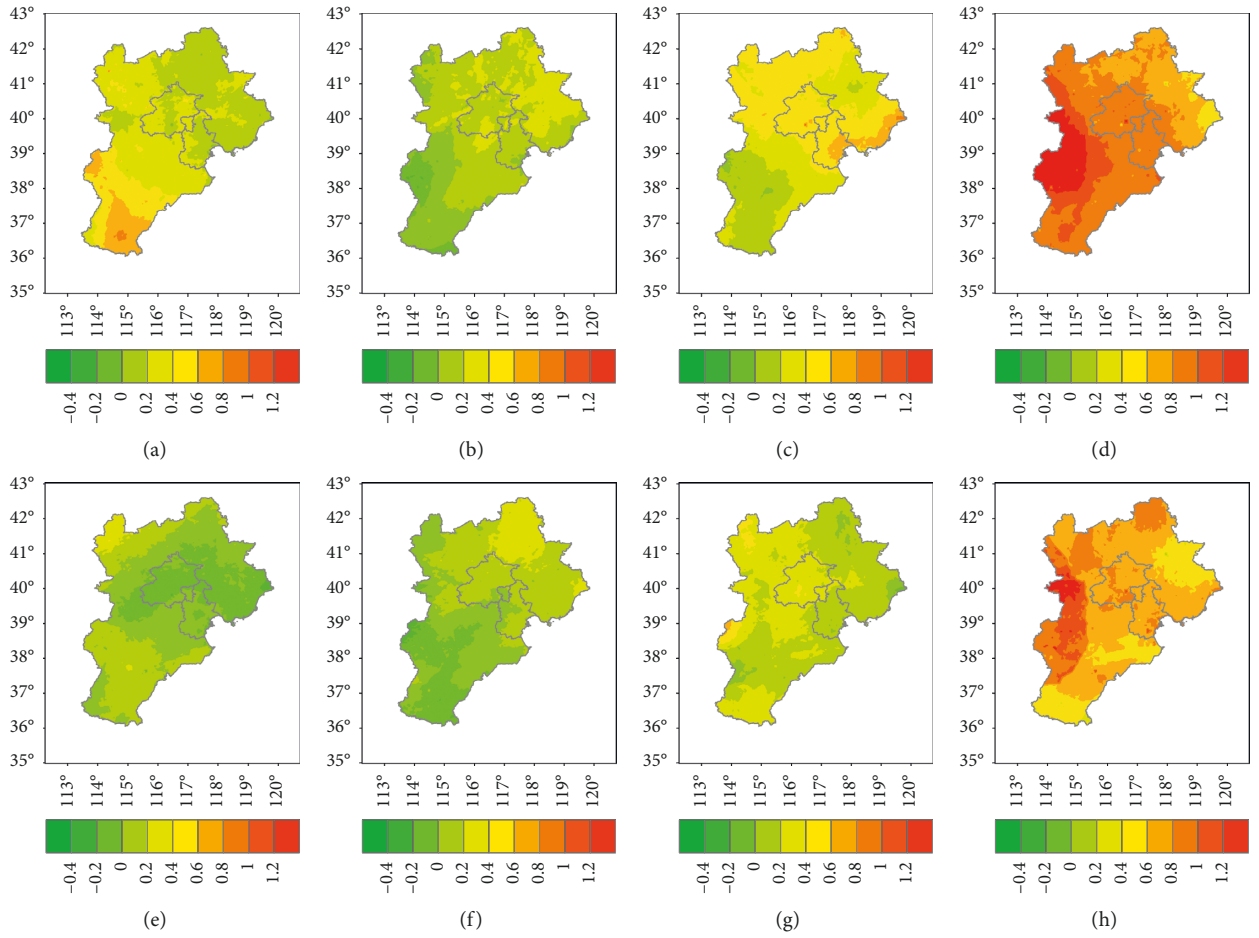

Figure 7: Interdecadal variations in mean temperature in spring and summer over the Beijing-Tianjin-Hebei region: (a) spring T2-T1; (b) spring T3-T2; (c) spring T4-T3; (d) spring T5-T4; (e) summer T2-T1; (f) summer T3-T2; (g) summer T4-T3; (h) summer T5-T4.

Figure 8 shows the spatial distribution of temperature changes over ten years in autumn and winter. From T1 to T2, the main warming areas in autumn and winter are distributed in the northwest, and most of the other areas mainly experience cooling temperatures, which are greater in winter than in autumn. In autumn from T2 to T3, the entire study area has a temperature increase between 0°C and 0.4°C. From T3 to T4, in some parts of the north and south areas and in Beijing, the temperature increases above 0.4°C. In winter, from T2 to T4, the Beijing-Tianjin-Hebei region experiences

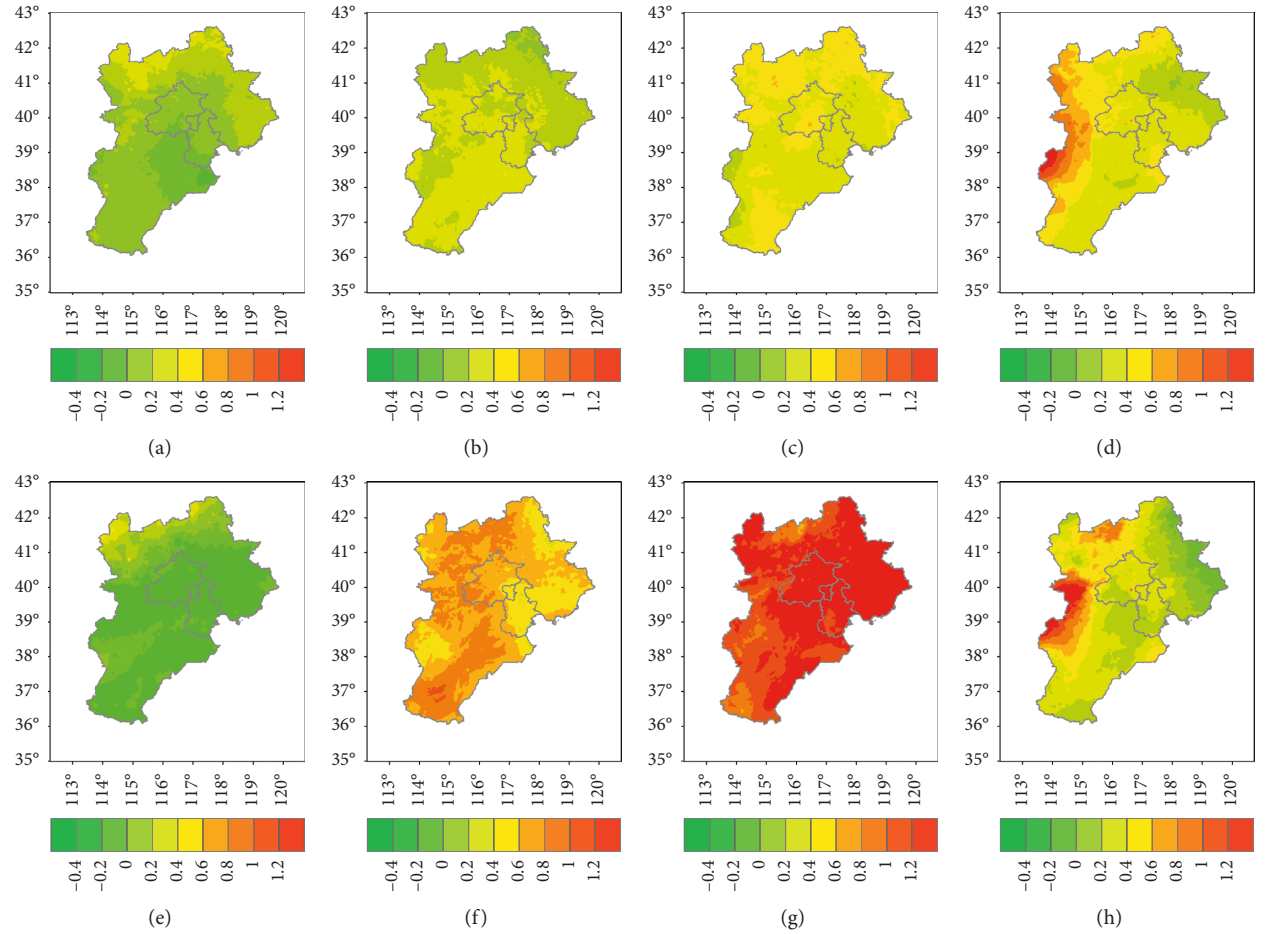

Figure 8: Interdecadal variations in mean temperature in autumn and winter over the Beijing-Tianjin-Hebei region: (a) autumn T2-T1; (b) autumn T3-T2; (c) autumn T4-T3; (d) autumn T5-T4; (e) winter T2-T1; (f) winter T3-T2; (g) winter T4-T3; (h) winter T5-T4.

intense heating, especially east of 115°E from T3 to T4, with the increase in temperature exceeding 1.2°C and the range of the warming zone reaching its maximum of the four seasons. The intensity is also the strongest. The four seasons from T4 to T5 show a similar spatial distribution of temperature changes, but most warming areas in autumn and winter warm to a lesser extent than those in spring and summer, and the northeast regions of the study areas become slightly cool. A small range of intense warming areas above 1.2°C also occurs in the western part of the study area in autumn and winter.

The annual temperature changes over multiple decades encompass the characteristics of the four seasons (Figure 9). From T1 to T2, the central part of the Beijing-Tianjin-Hebei region is mainly cooled, with weak warming in the south and northwest regions of the study area. Most of the areas from T2 to T3 warm up between 0.2°C and 0.4°C. From T3 to T4, the temperature increase is further aggravated, especially in the northwest and eastern regions of the study area and in Beijing and Tianjin, where the warming exceeds 0.6°C. From T4 to T5, the distribution characteristics of the increasing temperature from east to west during the four seasons reappear. West of the study area between 38°N and 40°N, the maximum temperature increase exceeds 1.2°C. Existing research [44, 45] has shown that, from the middle of the last century to the beginning of the 21st century, there has been strong warming of 0.5°C/10 yr in Zhangjiakou and Baoding, which are in the western part of the Beijing-Tianjin-Hebei region. This strong warming is also shown in the present study, and the location where it occurred is consistent with previous studies. In addition, we further confirm that this warming phenomenon occurred only since the late 1990s and exhibited no seasonal differences.

4. Conclusion

In this paper, HASM is applied as a data fusion tool to obtain high-precision simulated temperature fields in the Beijing-Tianjin-Hebei region using simulated fields from the regional numerical weather model as the approximate driving fields and observed data from the meteorological stations as the accuracy control points. The main conclusions of this paper are as follows:

(i) The WRF simulation of the temperature in the study area has relatively good accuracy, especially in summer and in the eastern part of the study area. However, due to the limitations of model

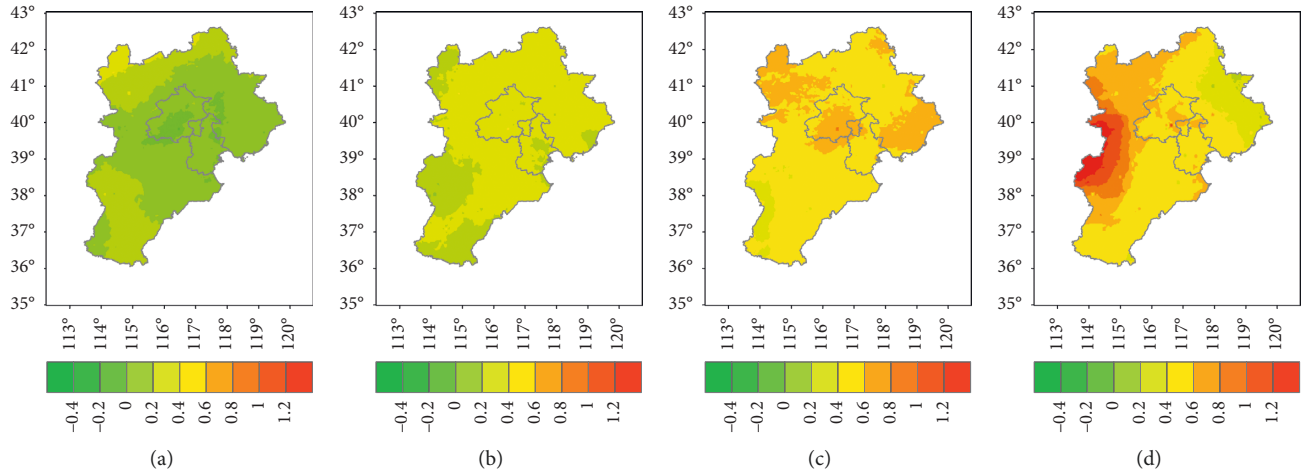

Figure 9: Interdecadal variations in mean temperature for the entire year over the Beijing-Tianjin-Hebei region: (a) T2-T1; (b) T3-T2; (c) T4-T3; (d) T5-T4.

performance, the overall deviation in the region is large. The spatial and temporal accuracies of the HASM-fused data are significantly higher than those of the WRF simulations. The warm bias of the WRF simulation is largely eliminated, reducing the MAEs and RMSEs by half in spring, autumn, and winter, and the SCC is increased by approximately 0.02. Increased accuracy makes the fusion data more suitable for long-term climate analysis. The increase in individual biases reflects the boundary problem of HASM.

(ii) The overall warming over 50 years is higher in spring and winter (0.039°C/yr and 0.056°C/yr, respectively), and the period from 1976 to 2005 is the period of rapid warming in the Beijing-Tianjin-Hebei region. Spring, summer, and autumn reached the highest heating rates in the last 10 years (from 1996 to 2005), while the winter warming period mainly occurred during the 1976–1995 period. The significant fluctuations in temperature between 1996 and 2005 in summer, autumn, and winter may be related to the frequent occurrence of extreme weather events.

(iii) In the first 40 years (1956–1995), the spatial distribution of temperature changes is significantly different among seasons and decades and does not reflect any notable distribution patterns. One similarity appears from 1996 to 2005, when the temperature rises dramatically in the western part of the study area in all four seasons. The annual mean temperature also exhibits this warming phenomenon from T4 to T5.

Fusing simulations from the WRF model with observations from stations increases the applicable area for HASM considering that the driving fields used to be generated through statistical approaches in previous studies of climate change. However, due to the long-term study period, the available meteorological stations are limited, which may cause uncertainty in the analysis of temperature changes and makes it difficult to study historical climate change. The results of this article reveal significant warming over the last three decades, which deserves further study. In future research, the study period could be shortened to increase the available observation sites and further improve the accuracy of the data fusion.

Data Availability

The data include (1) temperature records of 64 stations, which can be downloaded from http://data.cma.cn/, and (2) the data downscaled by the WRF model, which can be downloaded from https://rda.ucar.edu/datasets/ds316.1/.

Conflicts of Interest

The authors declare that there are no conflicts of interest.

Acknowledgments

This work was supported by the National Natural Science Foundation of China (41590844 and 41421001) and the Innovation Project of LREIS (O88RA600YA). We are grateful for the temperature observations from the National Meteorological Information Center, the 300 m annual global land cover dataset from the ESA, and the "NCAR CESM Global Bias-Corrected CMIP5 Output to Support WRF/MPAS Research" data from the NCAR.

References

[1] K. P. Shine and P. M. D. F. Forster, "The effect of human activity on radiative forcing of climate change: a review of recent developments," *Global and Planetary Change*, vol. 20, no. 4, pp. 205–225, 1999.

[2] Z. M. Ma, S. Z. Kang, L. Zhang, L. Tong, and X. L. Su, "Analysis of impacts of climate variability and human activity on streamflow for a river basin in arid region of northwest

China," *Journal of Hydrology*, vol. 352, no. 3-4, pp. 239–249, 2008.

[3] T. Kjellstrom, D. Briggs, C. Freyberg, B. Lemke, M. Otto, and O. Hyatt, "Heat, human performance, and occupational health: a key issue for the assessment of global climate change impacts," *Annual Review of Public Health*, vol. 37, no. 1, pp. 97–112, 2016.

[4] B. J. Harvey, "Human-caused climate change is now a key driver of forest fire activity in the western United States," *Proceedings of the National Academy of Sciences*, vol. 113, no. 42, pp. 11649-11650, 2016.

[5] IPCC-Intergovernmental Panel on Climate Change, *Climate Change 2013: The Physical Science Basis*, Cambridge University Press, Cambridge, UK, 2013.

[6] L. Chen and O. W. Frauenfeld, "Impacts of urbanization on future climate in China," *Climate Dynamics*, vol. 47, no. 1-2, pp. 345–357, 2016.

[7] R. Yu, X. S. Wang, Z. Yan, H. M. Yan, and Q. N. Jiang, "Regional climate effects of conversion from grassland to forestland in southeastern China," *Advances in Meteorology*, vol. 2013, Article ID 630953, 9 pages, 2013.

[8] D. B. Jiang, Y. Zhang, and X. M. Lang, "Vegetation feedback under future global warming," *Theoretical and Applied Climatology*, vol. 106, no. 1-2, pp. 211–227, 2011.

[9] J. Feng, J. Wang, and Z. Yan, "Impact of anthropogenic heat release on regional climate in three vast urban agglomerations in China," *Advances in Atmospheric Sciences*, vol. 31, no. 2, pp. 363–373, 2014.

[10] T. Economics, *China GDP Annual Growth Rate 1989–2018*, Trading Economics, New City, NY, USA, 2018.

[11] P. Gong, S. Liang, E. J. Carlton et al., "Urbanisation and health in China," *The Lancet*, vol. 379, no. 9818, pp. 843–852, 2012.

[12] Z. Zhang, X. Zhang, D. Gong, S.-J. Kim, R. Mao, and X. Zhao, "Possible influence of atmospheric circulations on winter haze pollution in the Beijing-Tianjin-Hebei region, northern China," *Atmospheric Chemistry and Physics*, vol. 16, no. 2, pp. 561–571, 2016.

[13] W. Cai, K. Li, H. Liao, H. Wang, and L. Wu, "Weather conditions conducive to Beijing severe haze more frequent under climate change," *Nature Climate Change*, vol. 7, no. 4, pp. 257–262, 2017.

[14] Z. Zhong, R. Huang, Q. Tang, X. Cong, and Z. Wang, "China's provincial CO_2 emissions embodied in trade with implications for regional climate policy," *Frontiers of Earth Science*, vol. 9, no. 1, pp. 77–90, 2015.

[15] Z. W. Yan, Z. Li, Q. X. Li, and P. Jones, "Effects of site change and urbanisation in the Beijing temperature series 1977–2006," *International Journal of Climatology*, vol. 30, no. 8, pp. 1226–1234, 2009.

[16] Z. Li and Z. W. Yao, "Homogenized daily mean/maximum/minimum temperature series for China from 1960–2008," *Atmospheric and Oceanic Science Letters*, vol. 2, no. 4, pp. 237–243, 2009.

[17] N. Zhao, N. Lu, C. Chen et al., "Mapping temperature using a Bayesian statistical method and a high accuracy surface modelling method in the Beijing-Tianjin-Hebei region, China," *Meteorological Applications*, vol. 24, no. 4, pp. 571–579, 2017.

[18] S. Miao, F. Chen, M. A. LeMone, M. Tewari, Q. Li, and Y. Wang, "An observational and modeling study of characteristics of urban heat island and boundary layer structures in Beijing," *Journal of Applied Meteorology and Climatology*, vol. 48, no. 3, pp. 484–501, 2009.

[19] X. Liu, G. Tian, J. Feng, B. Ma, J. Wang, and L. Kong, "Modeling the warming impact of urban land expansion on hot weather using the weather research and forecasting model: a case study of Beijing, China," *Advances in Atmospheric Sciences*, vol. 35, no. 6, pp. 723–736, 2018.

[20] D.-F. Zhang and Y. Shi, "Numerical simulation of climate changes over north China by the model RegCM3," *Chinese Journal of Geophysics*, vol. 55, no. 5, pp. 474–487, 2012.

[21] C. Talbot, E. Bou-Zeid, and J. Smith, "Nested mesoscale large-eddy simulations with WRF: performance in real test cases," *Journal of Hydrometeorology*, vol. 13, no. 5, pp. 1421–1441, 2012.

[22] D. Jacob, L. Bärring, O. B. Christensen et al., "An inter-comparison of regional climate models for Europe: model performance in present-day climate," *Climatic Change*, vol. 81, no. S1, pp. 31–52, 2007.

[23] N. Zhao, T. X. Yue, W. J. Shi, X. Zhou, Y. Liu, and Z. P. Du, "Downscaling simulation of annual average temperature and precipitation of CMIP5 outputs by using HASM—a case study in Heihe River basin," *Journal of Desert Research*, vol. 37, no. 6, pp. 1227–1236, 2017.

[24] T. X. Yue, N. Zhao, R. D. Ramsey et al., "Climate change trend in China, with improved accuracy," *Climatic Change*, vol. 120, no. 1-2, pp. 137–151, 2013.

[25] T. Yue, N. Zhao, Z. Fan et al., "CMIP5 downscaling and its uncertainty in China," *Global and Planetary Change*, vol. 146, pp. 30–37, 2016.

[26] J. Schmidli, C. M. Goodess, C. Frei et al., "Statistical and dynamical downscaling of precipitation: an evaluation and comparison of scenarios for the European Alps," *Journal of Geophysical Research: Atmospheres*, vol. 112, no. D4, pp. 1–20, 2007.

[27] T. X. Yue, *Surface Modeling: High Accuracy and High Speed Methods*, CRC Press, New York, NY, USA, 2011.

[28] M. S. Bukovsky and D. J. Karoly, "Precipitation simulations using WRF as a nested regional climate model," *Journal of applied Meteorology and Climatology*, vol. 48, no. 10, pp. 2152–2159, 2009.

[29] Y. Gao, J. Xu, and D. Chen, "Evaluation of WRF mesoscale climate simulations over the Tibetan plateau during 1979–2011," *Journal of Climate*, vol. 28, no. 7, pp. 2823–2841, 2015.

[30] C. L. Bruyere, J. M. Done, G. J. Holland, and S. Fredrick, "Bias corrections of global models for regional climate simulations of high-impact weather," *Climate Dynamics*, vol. 43, no. 7-8, pp. 1847–1856, 2014.

[31] B. H. Vaid, "Numerical simulations and analysis of June 16, 2010 heavy rainfall event over Singapore using the WRFV3 model," *International Journal of Atmospheric Sciences*, vol. 2013, Article ID 825395, 8 pages, 2013.

[32] V. A. Toponogov, *Differential Geometry of Curves and Surfaces*, Birkhaeuser Boston, New York, NY, USA, 2006.

[33] Y. Liu, T. Yue, L. Zhang, N. Zhao, M. Zhao, and Y. Liu, "Simulation and analysis of XCO_2 in North China based on high accuracy surface modeling," *Environmental Science and Pollution Research*, vol. 25, no. 27, pp. 27378–27392, 2018.

[34] W. J. Shi, J. Y. Liu, Z. P. Du, A. Stein, and T. X. Yue, "Surface modelling of soil properties based on land use information," *Geoderma*, vol. 162, no. 3-4, pp. 347–357, 2011.

[35] W.-J. Shi, T.-X. Yue, Z.-P. Du, Z. Wang, and X.-W. Li, "Surface modeling of soil antibiotics," *Science of the Total Environment*, vol. 543, pp. 609–619, 2016.

[36] Y. Wang, T. Yue, Y. Lei, Z. Du, and M. Zhao, "Uncertainty of forest biomass carbon patterns simulation on provincial scale:

a case study in Jiangxi Province, China," *Journal of Geographical Sciences*, vol. 26, no. 5, pp. 568–584, 2016.

[37] T. X. Yue, Y. Liu, M. W. Zhao, Z. P. Du, and N. Zhao, "A fundamental theorem of Earth's surface modelling," *Environmental Earth Sciences*, vol. 75, no. 9, p. 751, 2016.

[38] L. Zhang, T. Yue, J. Wilson et al., "Modelling of XCO_2 surfaces based on flight tests of TanSat instruments," *Sensors*, vol. 16, no. 11, p. 1818, 2016.

[39] L. L. Zhang, T. X. Yue, J. P. Wilson et al., "A comparison of satellite observations with the XCO_2 surface obtained by fusing TCCON measurements and GEOS-Chem model outputs," *Science of the Total Environment*, vol. 601-602, pp. 1575–1590, 2017.

[40] N. Zhao, T. Yue, H. Li, L. Zhang, X. Yin, and Y. Liu, "Spatio-temporal changes in precipitation over Beijing-Tianjin-Hebei region, China," *Atmospheric Research*, vol. 202, pp. 156–168, 2018.

[41] N. Zhao, T. X. Yue, X. Zhou et al., "Statistical downscaling of precipitation using local regression and high accuracy surface modeling method," *Theoretical and Applied Climatology*, vol. 129, no. 1-2, pp. 281–292, 2017.

[42] P. Zhai and X. Pan, "Trends in temperature extremes during 1951–1999 in China," *Geophysical Research Letters*, vol. 30, no. 17, 2003.

[43] J. Wang, D. K. Jiang, and Y. J. Zhang, "Analysis on spatial and temporal variation of extreme climate events in North China," *Chinese Journal of Agrometeorology*, vol. 33, no. 2, pp. 166–173, 2012.

[44] P. F. Li, W. J. Liu, and X. Y. Zhao, "The changes of atmospheric temperature, precipitation and potential evapotranspiration in Beijing-Tianjin-Hebei region in recent 50 years," *Journal of Arid Land Resources and Environment*, vol. 29, pp. 137–143, 2015.

[45] K. H. Zhang, J. F. Liu, F. Y. Liu, and S. R. Xiao, "Study on temporal and spatial characteristics of climate variation in Hebei area during 1956–2007," *Journal of Anhui Agricultural Sciences*, vol. 40, pp. 416–418, 2012.